The impact of high frequency rapid viral antigen screening on COVID-19 spread and outcomes: a validation and modeling study

Authors: Beatrice Nash[1,2*], Anthony Badea[1,3*], Ankita Reddy[1,4*], Miguel Bosch[1,5], Nol Salcedo[1], Adam R. Gomez[1], Alice Versiani[6], Gislaine Celestino Dutra Silva[6], Thayza Maria Izabel Lopes dos Santos[6], Bruno H. G. A. Milhim[6], Marilia M Moraes[6], Guilherme Rodrigues Fernandes Campos[6], Flávia Quieroz[6], Andreia Francesli Negri Reis[6], Mauricio L. Nogueira[6], Elena N. Naumova[7], Irene Bosch[1,8], Bobby Brooke Herrera[1,9†]

[*]These authors contributed equally to this work.

Affiliations:

[1]E25Bio, Inc., Cambridge, MA, USA

[2]Department of Computer Science, Harvard University School of Engineering and Applied Sciences, Cambridge, MA, USA

[3]Department of Physics, Harvard University, Cambridge, MA, USA

[4]Perelman School of Medicine, University of Pennsylvania, Philadelphia, PA, USA

[5]InfoGeosciences LLC, Houston, TX, USA

[6]Faculdade de Medicina de São José do Rio Preto (FAMERP), São José do Rio Preto, Brazil

[7]Division of the Nutrition Epidemiology and Data Science, Friedman School of Nutrition Science and Policy, Tufts University, Boston, MA, USA

[8]Department of Medicine, Mount Sinai School of Medicine, New York, NY, USA

[9]Department of Immunology and Infectious Diseases, Harvard T.H. Chan School of Public Health, Boston, MA, USA

[†]Corresponding Author. BBH, email: bbherrera@e25bio.com

Short Title: Modeling rapid antigen testing on COVID-19 spread

Abstract

High frequency screening of populations has been proposed as a strategy in facilitating control of the COVID-19 pandemic. Here we use computational modeling, coupled with clinical data from rapid antigen tests, to predict the impact of frequent rapid testing on COVID-19 spread and outcomes. Using patient nasal or nasopharyngeal swab specimens, we demonstrate that the sensitivity/specificity of two rapid antigen tests compared to quantitative real-time polymerase chain reaction (qRT-PCR) are 80.0%/91.1% and 84.7%/85.7%, respectively; moreover, sensitivity correlates directly with viral load. Based on COVID-19 data from three regions in the United States and São José do Rio Preto, Brazil, we show that high frequency, strategic population-wide rapid testing, even at varied accuracy levels, diminishes COVID-19 infections, hospitalizations, and deaths at a fraction of the cost of nucleic acid detection via qRT-PCR. We propose large-scale antigen-based surveillance as a viable strategy to control SARS-CoV-2 spread and to enable societal re-opening.

INTRODUCTION

The COVID-19 pandemic has taken an unprecedented toll on lives, wellbeing, healthcare systems, and global economies. As of 4 November 2020, there have been more than 47.6 million confirmed cases globally with more than 1 million confirmed deaths (*1*). However, these numbers and the current mapping of disease spread present an incomplete picture of the outbreak largely due to the lack of adequate testing, particularly as undetected infected cases are the main source of disease spread (*2–7*). It is estimated that the reported detection rate of actual COVID-19 cases is only 1-2% (*5*). As of November 2020, the United States, Brazil, and India remain the top three countries with the highest number of COVID-19 cases and deaths worldwide. As countries begin to re-open their economies, a method for accessible and frequent surveillance of COVID-19, with the necessary rapid quarantine measures, is crucial to prevent the multiple resurgences of the disease.

The current standard of care rightfully places a strong focus on the diagnostic limit of detection, yet frequently at the expense of both cost and turnaround time. This situation has contributed to limited population testing largely due to a dearth of diagnostic resources. Quantitative real-time polymerase chain reaction (qRT-PCR) is the gold-standard method for clinical diagnosis, with high sensitivity and specificity, but these tests are accompanied by the need for trained personnel, expensive reagents and instrumentation, and a significant amount of time to execute. Facilities offering qRT-PCR sometimes require a week or longer to complete and return the results to the patient. During this waiting period the undiagnosed individual may spread the infection and/or receive delayed medical treatment. Moreover, due to the cost and relative inaccessibility of qRT-PCR in both resource-limited and abundant settings, large-scale screening using qRT-PCR at frequent intervals remains impractical to identify infected but asymptomatic or

92 mildly symptomatic infections. Numerous studies have reported asymptomatic COVID-19 cases
93 as well as a variation in viral load within and between individuals at different time points,
94 suggesting the need for more frequent testing for informative surveillance.

95 Technologies alternate to qRT-PCR, such as rapid viral antigen detection, clustered
96 regularly interspaced short palindromic repeats (CRISPR), and loop-mediated isothermal
97 amplification (LAMP) of SARS-CoV-2 provide potential large-scale screening applications, yet
98 their implementation is stymied by requirements for qRT-PCR-like accuracy before they can reach
99 the market (*8*). In countries such as India, where the qRT-PCR resources would not be sufficient
100 to cover monitoring of the population, the use of rapid antigen tests is well underway(*9*, *10*). In
101 early May 2020, the United States Food and Drug Administration (FDA) authorized the first
102 antigen test for the laboratory detection of COVID-19, citing a need for testing beyond molecular
103 and serological methods. Antigen testing detects the viral proteins rather than nucleic acids or
104 human antibodies, allowing for detection of an active infection with relative ease of sample
105 collection and assay. These rapid assays – like other commercially-available rapid antigen tests -
106 can be mass-produced at low prices and be administered by the average person without a laboratory
107 or instrumentation. These tests also take as little as 15 minutes to determine the result, enabling
108 real-time surveillance and/or diagnosis. Although antigen tests usually perform with high
109 specificities (true negative rate), their sensitivity (true positive rate) is often lower when compared
110 to molecular assays. While qRT-PCR can reach a limit of detection as low as 10^2 genome copies
111 per mL, rapid antigen testing detects viral protein that is assumed to correlate with approximately
112 10^5 genome copies per mL (*11*).

113 We hypothesize that frequent antigen-based rapid testing even with lower sensitivities
114 compared to qRT-PCR - along with appropriate quarantine measures - can be more effective at

115 decreasing COVID-19 spread than less frequent molecular testing of symptomatic individuals.
116 Keeping in mind the realities of daily testing in resource-limited regions, we also hypothesize that
117 testing frequency can be adjusted according to the prevalence of the disease; that is, an uptick in
118 reported cases should be accompanied by more frequent testing. During the viral incubation period,
119 high infectivity correlates with a high viral load that can be detected by either qRT-PCR or rapid
120 antigen testing (*12–16*). Rapid tests thus optimize diagnosis for the most infectious individuals.
121 Studies also point to the relatively small window of time during an individual's incubation period
122 in which the qRT-PCR assay is more sensitive than rapid tests (*12*).

123 In this study we report the clinical validation of two direct antigen rapid tests for detection
124 of SARS-CoV-2 spike glycoprotein (S) or nucleocapsid protein (N) using retrospectively collected
125 nasopharyngeal or nasal swab specimens. Using the clinical performance data, we develop a
126 modeling system to evaluate the impact of frequent rapid testing on COVID-19 spread and
127 outcomes using a variation of a SIR model, which has been previously used to model COVID-19
128 transmission (*17–23*). We build on this model to incorporate quarantine states and testing protocols
129 to examine the effects of different testing regimes. This model distinguishes between undetected
130 and detected infections and separates severe cases, specifically, those requiring hospitalization,
131 from those less so, which is important for disease response systems such as intensive care unit
132 triaging. We simulate COVID-19 spread with rapid testing and model disease outcomes in three
133 regions in the United States and São José do Rio Preto, Brazil - the site of the clinical validation
134 study - using publicly available data. To date, COVID-19 modeling describes the course of disease
135 spread in response to social distancing and quarantine measures, and a previous simulation study
136 has shown that frequent testing with accuracies less than qRT-PCR, coupled with quarantine
137 process and social distancing, are predicted to significantly decrease infections (*12*, *17*, *23–27*).

138 This is the first modeling system using publicly-available data to simulate how potential public
139 health strategies based on testing performance, frequency, and geography impact the course of
140 COVID-19 spread and outcomes. Our findings suggest that a rapid test, even with sensitivities
141 lower than molecular tests, when strategically administered 2-3 times per week, will reduce
142 COVID-19 spread, hospitalizations, and deaths at a fraction of the cost of nucleic acid testing via
143 qRT-PCR. Modern surveillance systems should be well equipped with rapid testing tools to ensure
144 that disease tracking and control protocols are effective and well-tailored to national, regional, and
145 community needs.
146

147 **RESULTS**

148 **Accuracy of Direct Antigen Rapid Tests Correlate with Viral Load Levels**

149 Rapid antigen tests have recently been considered a viable source for first-line screening,
150 although concerns about the accuracy of these tests persist. We clinically validated two different
151 direct antigen rapid tests for the detection of either N or S from SARS-CoV-2 in retrospectively
152 collected nasal or nasopharyngeal swab specimens. Of the total number of nasal swab specimens
153 evaluated by qRT-PCR for amplification of SARS-CoV-2 N, S, and ORF1ab genes, 100 tested
154 positive and 90 tested negative (Table 1, Table S1). The overall sensitivity and specificity of the
155 rapid antigen test for detection of SARS-CoV-2 N, evaluated across the nasal swab specimens,
156 was 80.0% and 91.1%, respectively. Of the total number of nasopharyngeal swab specimens
157 evaluated by qRT-PCR for amplification of SARS-CoV-2 N, RNA-dependent RNA polymerase
158 (RdRp), and envelope (E) genes, 72 tested positive and 49 tested negative (Table 2, Table S1). The
159 overall sensitivity and specificity of the rapid antigen test for detection of SARS-CoV-2 S,
160 evaluated across the nasopharyngeal swab specimens was 84.7% and 85.7%, respectively.

161 Altogether, our data demonstrate that the sensitivity of the rapid antigen tests are positively
162 correlated to the viral load level (Table S1).

163 The Ct value indirectly quantifies the viral RNA copy number related to the viral load of
164 the sample for the specific assay (*28*, *29*). Ct values represent the number of qRT-PCR cycles at
165 which generated fluorescence crosses a threshold during the linear amplification phase; Ct values
166 are therefore inversely related to the viral load. The sensitivity of both rapid antigen tests increases
167 as Ct value decreases (Table S1). Moreover, because the Ct value is a variable unit based upon
168 qPCR protocol and instrumentation, we evaluated sensitivity against the percentile of positive
169 cases conditioned to Ct and found similar results. The sensitivity of the rapid antigen test for
170 detection of SARS-CoV-2 N increased from 80.0% at Ct values <40 to 95.8% at Ct values <20
171 (Figure S1A). Similarly, the sensitivity of the rapid antigen test for detection of SARS-CoV-2 S
172 increased from 84.7% at Ct values <35 to 100.0% at Ct values <15 (Figure S1B). Taken together,
173 the clinical data shows that the rapid antigen test performs with increasing accuracy for individuals
174 with a higher viral load, and potentially the most infectious (*13–16*).

175

176 **An Enhanced Epidemiological SIDHRE-Q Model**

177 We propose an enhanced epidemiological modeling system, *SIDHRE-Q,* a variant of the
178 classical SIR model in order to expand our clinical validation study and to understand the effects
179 of using frequent rapid tests such as the rapid antigen test on COVID-19 outbreak dynamics. The
180 changes we make to the basic model to encompass the unique characteristics of the COVID-19
181 pandemic are similar to those presented by Giordano et al. *(16)* (Figure 1, Figure S2). The
182 differential equations governing the evolution of the *SIDHRE-Q* model and descriptions of the
183 parameter values are provided in the material and methods section (Equation 2, Table 3).

An individual that begins in **S** may either transition to a Quarantine Uninfected (**Q-U**) state via a false positive result or to an Infected Undetected (**I**) state via interaction with an infected individual. Should an individual in **S** move into **Q-U**, they are quarantined for 14 days before returning to **S**, a time period chosen based on current knowledge of the infectious period of the disease. One could also conceive of an effective strategy in which individuals exit quarantine after producing a certain number of negative rapid tests in the days following their initial positive result or confirm their negative result using qRT-PCR.

Given that those diagnosed are predominantly quarantined, individuals in **I** interact more with the **S** population than do those in Infected Detected (**D**). Therefore, the infectious rate for **I** is assumed to be significantly larger than for **D**. Furthermore, a region's ability to control an outbreak is directly related to how quickly and effectively people in **I** test into **D**, reducing their infectiousness through quarantine. This study, in particular, highlights the critical role frequency of testing, along with strict quarantine, has in mitigating the spread of the disease and provides specific testing strategies based on rapid tests we predict to be highly effective.

In this model, we assume that individuals receive a positive diagnosis before developing severe symptoms and that those with symptoms severe enough to be potentially fatal will go to the hospital. If an individual develops symptoms, we assume they are tested daily until receiving a positive result; hence, before severe symptoms develop, they will be diagnosed with high probability. Those who do not develop symptoms are tested according to the frequency of tests administered to the general population. Therefore, there is no modeled connection between **I** and **H** or between **I** and **E**. Removing these assumptions would have negligible impact on the results as these flows are very small.

Should an individual test positive and transition to **D**, they may either develop serious symptoms requiring care or recover. Those who develop serious symptoms and transition to state **H** will then transition to either **R** or **E**. The recovered population is inevitably tested, as infected individuals may recover without being detected. Therefore, the Quarantined Recovered (**Q-R**) state is introduced with the same connections to **R** as the connections between **S** and **Q-U**. Though the reinfection rate of SARS-CoV-2 has been a point of recent debate, it is assumed that the number of re-infected individuals is small (*30–34*). Therefore, individuals cannot transition from **R** to **S**, hence the separately categorized quarantined populations.

We considered several variations and extensions of the *SIDHRE-Q* model. In simulations, we tested additional states, such as those in the *SIDARTHE* model, which include distinctions between symptomatic and asymptomatic cases for both detected and undetected populations (*17*). Incorporating information about the correlations between viral load and infectivity and sensitivity were also considered. Altogether, our modeling system has been well tuned to predict the impact of high frequency rapid testing on COVID-19 spread and outcomes.

Frequent Rapid Testing with Actionable Quarantining Dramatically Reduces Disease Spread

In order to demonstrate how strategies could affect the disease spread in different geographies and demographics, we used surveillance data obtained from regions of varying characteristics: the state of Massachusetts (MA), New York City (NYC), Los Angeles (LA), and São José do Rio Preto (SJRP), Brazil, the site of the rapid antigen test clinical validation study. These regions are also selected in our study due to the readily available surveillance data provided by the local governments. We fit the model to the data from each region starting 1 April 2020. At

229 this time point the disease reportedly is most advanced in NYC and least advanced in SJRP, Brazil
230 with estimated cumulative infection rates of 7.11% and 0.12%, respectively.

231 After calibrating the *SIDHRE-Q* model, the disease spread is observed with varying
232 validated rapid antigen test performances and frequencies (Figure 2A). Sensitivity (the ratio of true
233 positives to the total number of positives) and specificity (the ratio of true negatives to the total
234 number of negatives) compared to gold-standard qRT-PCR were used as measures of test
235 accuracy.

236 The rapid test frequency is varied while maintaining an accuracy of 80% sensitivity and
237 90% specificity, comparable to our clinical data collected in SJRP, Brazil. These testing scenarios
238 are then compared to symptomatic testing, in which individuals receive a rapid test only when
239 presenting symptoms, via either a rapid test or qRT-PCR. Since the primary testing regiment
240 deployed in MA, LA, NYC and SJRP, Brazil is qRT-PCR-based and focused on symptomatic
241 individuals, the symptomatic testing protocol via qRT-PCR is directly estimated from the data to
242 be the rate ν (Table 3).

243 The difference between the qRT-PCR and rapid test simulations (red and orange lines,
244 respectively) is therefore only sensitivity of testing (Figure 2A). We assumed that test outcome
245 probability is a function only of whether an individual is infected and independent of other factors;
246 one can consider this a lower bound on effectiveness of a strategy, as sensitivity and infectivity
247 are often positively correlated with antigen testing.

248 To better understand the effect of rapid testing frequency and performance on healthcare
249 capacity and mortality rates, we simulate the testing strategy with 30%-90% sensitivity each with
250 80% or 90% specificity against the symptomatic testing strategy (Figure S3).

251 As per our hypothesis, frequency and symptom-based testing dramatically reduced
252 infections, simultaneous hospitalizations, and total deaths when compared to the purely symptom-
253 based testing regiments, and infections, hospitalization, and death were reduced as frequency
254 increased. Although testing every day was clearly most effective, even testing every fourteen days
255 with an imperfect test gave an improvement over symptomatic testing with qRT-PCR. While the
256 strategy works best when implemented at the very beginning of an outbreak, as demonstrated by
257 the results in SJRP, Brazil, it also works to curb an outbreak that is already large, as demonstrated
258 by the results in NYC. The difference between frequencies is more noticeable when the testing
259 strategy is applied to the outbreak in NYC, leading us to hypothesize that smaller outbreaks require
260 a lower testing frequency than larger ones; note the difference between the dependence on
261 frequency to curb a small initial outbreak in SJRP, Brazil versus a large one in NYC (Figure 2B).

262 For test performance of 80% sensitivity and 90% specificity, the percent of the population
263 that has been infected in total from the beginning of the outbreak to mid-July drops from 18%
264 (MA), 11% (LA), 26% (NYC), and 11% (SJRP, Brazil) to 3%, 2%, 12%, and 0.26%, respectively,
265 using a weekly rapid testing and quarantine strategy (with regards to predictions of overall
266 infection rates, other studies based on seroprevalence and epidemiological predictions have
267 reached similar conclusions (*35*, *36*)). If testing is increased to once every three days, these
268 numbers drop further to 1.6% (MA), 1.4% (LA), 9.4% (NYC), and 0.19% (SJRP, Brazil) (Table
269 S2).

270 To further examine the relationship between frequency and sensitivity, we modeled the
271 maximum number of individuals in a given state over the 105-day time period for four geographic
272 regions (Figure 2B, Figure S4). In all four geographic regions, as frequency of testing increases,
273 the total infections, maximum simultaneous hospitalizations, and total deaths converge to small

274 percentages regardless of the sensitivity at high frequencies. It is clear that the difference in
275 frequency required to achieve the same result using tests of differing sensitivities is very small.
276 For example, we predict that for the outbreak in LA, a testing strategy started on 1 April of every
277 10 days using a test of sensitivity 90% would have resulted in 2.5% of the population having been
278 infected, while using a test of sensitivity 30% would require a strategy of every 5 days to achieve
279 the same number. Thus, we conclude that frequency is more important than sensitivity in curbing
280 the spread, and a large range of sensitivities prove effective when testing sufficiently often (Figure
281 S4). How frequently, exactly, depends on the specific outbreak and what stage it is in, which leads
282 us to the location-based deployment strategy discussed in a later section. Frequency of testing can
283 be significantly reduced to effectively contain the disease once the initial outbreak has been
284 controlled; it is clear that this takes only a matter of weeks (Figure 2A).

285 On the other hand, according to the specificity of the rapid test and the quarantine duration,
286 larger testing frequency result in a larger percent of the population quarantined (Figure 2A).
287 Assuming a 90% rapid test specificity and 14-day quarantine duration, for the 1-, 3- and 7-day
288 frequencies almost 60%, 38% and 20% of the population, respectively, would be quarantined. This
289 figure may be reduced with additional rules for exiting quarantine early, such as after
290 complementary testing. An example of such a strategy is that individuals who test positive are
291 required to either quarantine for two weeks or produce two consecutive negative rapid tests in the
292 two days following their positive result. Assuming 80% sensitivity and 90% specificity, those
293 individuals will reenter the public while still infected with probability 0.04. If uninfected, that
294 individual will exit quarantine after two days with probability 0.81. However, a compromise
295 between the reduction of infections and the proportion of the population in quarantine would be
296 part of the planning for the appropriate testing protocol in each community or region.

Additionally, while high frequency may be necessary to contain a large outbreak initially, relatively infrequent testing, such as every one or two weeks, is sufficient to keep controlled outbreaks small, while reducing the number of quarantined individuals to less than 10% of the population using a two-week mandatory quarantine.

A County-Based Testing Strategy Offers a Cost-effective Approach to Large-scale COVID-19 Surveillance

To examine the effects of resource-strategic testing schemes, we modeled the COVID-19 prevalence by varying testing frequency across counties of California. For this analysis, only California was analyzed because of the accessibility of the county level data and the variability of spread dynamics of the outbreaks between counties. In this scheme, the percent of active infected detected individuals in a county determines the frequency of testing. We define thresholds for the number of active detected infections that, when hit, initiate testing protocols of different frequencies depending on the threshold hit. We first tested evenly spaced thresholds for the number of detected active infections up to 1% of the population, but later adopted thresholds that were determined according to Equation 1. In Equation 1, D = population of state **D** at the time of testing. T = number of active infections which, if reached, initiates everyday testing. The days between tests are rounded to the closest integer value.

$$\text{Days between tests} = \max\left(1, 2\log_2(T/D) + 1\right) \tag{1}$$

The days between tests are chosen such that the detected active infections should remain near to or below T. If the initial detected active infections are greater than T, then the testing frequency of 1 will cause infections to rapidly drop. Both the threshold at which everyday testing begins and

320 the coefficient of $log_2 T/D$ can be modified to produce a strategy that is more or less frequent in
321 testing or resource effective; a range of days between tests from 14 days to 1 day are used (Figure
322 3A). The purpose of this strategy is to tailor testing based on the specific characteristics of local
323 outbreaks in order to mitigate the overall spread faster and more efficiently. A scan over different
324 choices of T is shown in Figure 3B; the threshold we choose in Figure 3A is 0.05% because it is
325 successful in curbing the outbreak within the time period we consider. While the choices work for
326 the epidemic in California at the point we start our simulations, 10 April, they do not necessarily
327 reflect the most resource effective choices everywhere. Our analysis could be redone to select the
328 best fine-grained strategy in other states or metropolitan areas.

329 Using a rapid test with a sensitivity of 80% and specificity of 90%, the county-based testing
330 with threshold 0.05% reduces the active infections from 0.94% to 0.0005%, while the uniform
331 strategy with tests administered every 7 days results in double the number of active infections
332 (Figure 3A). As the threshold is reduced, the total cost increases while the cumulative infections,
333 maximum percentage hospitalized, and cumulative deaths all decrease (Figure 3B). Appropriate
334 choice of threshold is dependent on the severity of outbreaks in a specific region and available
335 resources, both logistically and fiscally. With regional data, such as that from California used to
336 produce Figure 3B, this study can be reproduced to calculate an efficient testing strategy that will
337 effectively curb outbreaks of differing severities in any geographic entity.

338 Strategy B in Figure 3 consists of qRT-PCR testing uniformly applied to the highlighted
339 population with a frequency of once weekly. The average cost per person per day is just under $15.
340 Despite this frequency and the accuracy of qRT-PCR, the strategy does not succeed in curbing the
341 spread as fast as strategy A, which uses a testing sensitivity and specificity of 80% and 90%,
342 respectively, and testing frequency that vary between counties depending on the proportion of their

343 population that is currently infected. The total cost for strategy A is estimated at a fraction of the
344 other at $1.53 per person per day.
345
346 **DISCUSSION**
347 In this study we examine the potential effects of a novel testing strategy to limit the spread
348 of SARS-CoV-2 utilizing rapid antigen test screening approaches. Our clinical data and *SIDHRE-*
349 *Q* modeling system demonstrate that 1) frequent rapid testing even at a range of accuracies is
350 effective at reducing COVID-19 spread, 2) rapid antigen tests are a viable source for this strategy
351 and diagnose the most infectious individuals, and 3) strategic geographic-based testing can
352 optimize disease control with the amount of available resources. The information from a diagnostic
353 test itself is of tremendous value, as it can prompt the necessary quarantine measures to prevent
354 spread, guide proper care and triage, and provide crucial disease-tracking information. Diagnostic
355 testing in the United States and abroad, however, has been a significant public health hurdle. The
356 public has witnessed and experienced symptomatic individuals being denied testing due to
357 shortages, and few testing structures for asymptomatic or mildly symptomatic individuals – a
358 significant source of disease spread. Though several factors contributed to the stymied early
359 response measures, such as lockdown and quarantine protocols and adherence, severe testing
360 bottlenecks were a significant culprit (*37–39*). Early control measures have been shown to decrease
361 lives lost by several orders of magnitude (*40*). These challenges, though exacerbated during the
362 early months of the pandemic, remain at the forefront of the public health crises.
363 Diagnosis of SARS-CoV-2 infection by qRT-PCR is the current standard of care, yet
364 remains expensive and requires a laboratory and experienced personnel for sample preparations
365 and experimentation. Significantly, the turnaround time for results can be up to 10 days (*41*). On
366 an individual scale, this leaves the public in limbo, preventing people from either leaving

367 quarantine if they are negative, or delaying critical care and infecting others if they are positive.
368 On a societal level, this current testing scheme yields incomplete surveillance data on which
369 response efforts such as societal reopening and hospital management depend. Though qRT-PCR
370 is considered the gold-standard diagnostic method because of its high sensitivity and specificity,
371 the logistical hurdles render it unrealistic for large-scale screening.

372 As qRT-PCR remains impractical for this strategy, and rapid tests are facing regulatory
373 challenges because they do not perform with qRT-PCR-like accuracy, rapid test screening is either
374 nonexistent in several countries or symptom-based. Even under best-case assumptions, findings
375 have shown that symptom and risk-based screening strategies miss more than half of the infected
376 individuals (*42*). Some have argued that the need for widespread testing is overstated due to the
377 variability in test sensitivity and specificity (*43*). Here, we present alternative large-scale
378 diagnostic tools to qRT-PCR, and show that test performance, though valuable, is secondary to
379 widespread test frequency, which is enabled by accessibility and turnaround time. Furthermore,
380 test affordability is essential for the successful implementation in communities most affected by
381 infection and will to speed up the safe opening and functioning of the viral sectors of the economy.

382 Giordano et al. has modeled the evolution of SARS-CoV-2 spread, introducing a diagnosed
383 state to elucidate the importance of population-wide testing (*17*). Mina et al. has examined how
384 various test sensitivities and frequencies affect the reproductive number (*12*). We build upon these
385 findings to show how in affected United States and Brazil regions, population-wide frequent and
386 rapid testing schemes, with sensitivities ranging from 30%-90%, can be more effective in curbing
387 the pandemic than a PCR-based scheme. Integrating real-world surveillance and clinical data into
388 our modeling system has allowed us to incorporate regional differences - such as variances in
389 healthcare access, state health policy and adherence, state GDP, and environmental factors - under

390 the same model. Significantly, our findings hold true across Massachusetts, New York City, Los
391 Angeles, and São José do Rio Preto, Brazil. We also present the economic considerations of these
392 testing regimes, showing that widespread rapid testing is more cost efficient than less frequent
393 qRT-PCR testing. In line with these economic considerations, our model demonstrates the
394 effectiveness of a geographic-based frequent testing regime, in which high disease prevalence
395 areas receive more frequent testing than low disease prevalence areas.

396 Since COVID-19 is known to affect certain demographics differently, modeling would
397 benefit from incorporating demographic information correlated with disease progression and
398 spread to define sub-models and sets of parameters accordingly. Age, pre-existing conditions, job
399 types, and density of population are examples of possible categories, each of which influence the
400 risk of contracting and/or dying from COVID-19. Further studies would benefit from incorporating
401 these ideas to better understand the effectiveness of rapid testing on identifying potential super
402 spreading events. Future public health prevention programs should use the proposed modeling
403 system to develop and test scenarios for precision testing and prevention.

404 Our findings also point to low-cost tools for implementation of this testing strategy, such
405 as a rapid antigen-based test for the detection of SARS-CoV-2 proteins. We show that the rapid
406 antigen tests perform with a range of accuracies under which disease spread can be dramatically
407 mitigated under our model. Notably, the sensitivity is correlated to the individual's viral load,
408 effectively diagnosing those who are potentially the most infectious with the highest accuracy. Our
409 findings are significant because rapid antigen tests are cheaper than qRT-PCR, can be mass
410 produced to millions per day, present results within 15 minutes, and can be administered by a
411 nonexpert without a lab or special equipment.

412 There are several policy implications for these findings. First, our model supports that
413 systems of high frequency rapid testing should be implemented as a first-line screening method.
414 This can be first enabled by a more holistic regulatory evaluation of rapid diagnostics, such that
415 policy emphasizes accessibility and turnaround time even under a range of accuracies. One can
416 imagine a less accurate, though rapid method of first-line screening in schools, public
417 transportation, and airports, or even at home, and a qRT-PCR-based method for second-line
418 screening (testing those who present severe symptoms or have been in contact with infected
419 individuals, testing in a clinical setting, etc). Second, our cost analysis and rapid antigen test data
420 present a viable and potentially more cost-effective method for screening. Third, our county-based
421 testing scheme presents a possible method for wide-scale screening while optimizing resources.
422 Future studies should investigate how this selective testing strategy can be applied to different
423 location scales to further inform health policy. Moreover, though our models analyze regions in
424 the United States and Brazil, similar testing strategies can be considered globally in both resource
425 limited and abundant settings due to the higher accessibility of rapid tests compared to qRT-PCR.
426 We emphasize that integral to the effectiveness of diagnostic schemes is 1) the proper
427 adherence to quarantine measures and 2) the combined use of a variety of diagnostic methods
428 including nucleic acid, antigen, and antibody tests. According to these models, rapid antigen tests
429 are an ideal tool for first-line screening. Clinical molecular tests such as qRT-PCR are vital to the
430 diagnostic landscape, particularly to re-test suspected cases that were negative on the rapid test.
431 Because rapid tests present a higher rate of false negatives, methods such as qRT-PCR remain
432 integral to second-line screening. Antibody tests provide important information for immunity and
433 vaccination purposes as well as epidemiological surveillance. This model also assumes that

434 individuals will quarantine themselves before being tested and for 14 days following a positive
435 diagnostic result.

436 Our simulations combined with real-world data demonstrate a robust modeling system and
437 elucidates the significance of this novel testing strategy. However, there are important limitations
438 to be considered. Differences in disease reporting between the geographical regions and the
439 incomplete nature of COVID-19 surveillance data, often due to the lack of testing, are not
440 considered in the model. It is imperative that the testing results, hospitalization and death statistics,
441 and changes in protocol are reported in real-time to scientists and policy makers so that models
442 can be accurately tuned as the pandemic develops. The model also does not take into account
443 infrastructural limitations such as hospital capacity. Though the rapid antigen test offers several
444 advantages such as affordability, fast turnaround time, and ease of mass production, we are also
445 assuming that there are systems in place to implement frequent and safe low-cost screening across
446 different communities and settings.

447 Our model underscores the need for a point-of-care or at-home test for frequent screening,
448 particularly as lockdown restrictions ease. Regulatory agencies such as the FDA could work
449 towards regulating rapid tests to alternative standards other than comparison to high sensitivity
450 molecular diagnostics, as our model shows that frequency and scale of testing may overcome lower
451 sensitivities. Rather, we could refocus policy to implement first-line screening that optimizes
452 accuracy with efficiency and equitability.

453

454

455

456

457 **MATERIAL AND METHODS**

458 **Development of Direct Antigen Rapid Tests for the Detection of SARS-CoV-2**

459 We developed a direct antigen rapid test for the detection of the nucleocapsid protein or
460 spike glycoprotein from SARS-CoV-2 in nasal or nasopharyngeal swab specimens as previously
461 described (*44*). Briefly, the rapid antigen tests are immunochromatographic format with a visual
462 readout using anti-N or anti-S mouse monoclonal antibodies (E25Bio, Inc., Cambridge, MA, USA)
463 that are either coupled to 40 nm gold nanoparticles (Abcam, Cambridge, UK) or adsorbed to
464 nitrocellulose membranes (Sartorius, Goettingen, Germany). Each rapid antigen test has a control
465 area adjacent to the paper absorbent pad; the control is an anti-mouse Fc domain antibody (Leinco
466 Technologies, Fenton, MO, USA) that will capture any of the antibody-conjugated gold
467 nanoparticles to generate a control visual signal. A visual signal at the test area reflects SARS-
468 CoV-2 N or S that is "sandwiched" between an anti-N or anti-S antibody adsorbed to the
469 nitrocellulose membrane and a second anti-N or anti-S antibody covalently coupled to visible gold
470 nanoparticles.

471

472 **Validation of Direct Antigen Rapid Test for the Detection of SARS-CoV-2**

473 In a retrospective study of nasal swab specimens form human patients, we compared the
474 accuracy of the rapid antigen test for detection of SARS-CoV-2 N to the viral loads of individuals.
475 Nasal swab specimens (n=190) were tested following approved human subjects use protocols. The
476 nasal swab specimens were banked frozen from suspected patients submitted to PATH for routine
477 COVID diagnosis. Prior to using the rapid test, the nasal swab specimens were validated by qRT-
478 PCR using the FDA EUA ThermoFisher/AppliedBiosystems TaqPATH COVID-19 Combo Kit
479 (ThermoFisher, Waltham, MA USA). The primary study under which the samples and data were

480 collected received ethical clearance from the PATH Research Ethics Committee, protocol number
481 00004244. The nasal swab specimens were de-identified, containing no demographic data, prior
482 to analysis.

483 The nasal swabs were originally collected in 1 mL PBS, where 50 µl was mixed with 50 µl
484 of Solution Buffer (0.9% NaCl and 0.1% Triton X-100). The 100 µl mixture was then pipetted
485 onto the rapid antigen test for SARS-CoV-2 nucleocapsid detection and allowed to react for 15
486 minutes. After processing of the rapid antigen test, the visual positive or negative signal was
487 documented.

488 Additionally, in a retrospective study of nasopharyngeal swab specimens from human
489 patients, we compared the accuracy of the rapid antigen test to the viral load of individuals.
490 Nasopharyngeal swab specimens (n = 121) were tested in Brazil following approved human
491 subjects use protocols. The age of study participants ranged from 1 to 95 years with an overall
492 median of 37 years (interquartile range, 27–51 years), and 62% were female. The demographic
493 summary of the patients are included in Table S3. The nasopharyngeal swab specimens were
494 banked refrigerated or frozen samples from suspected patients submitted to the lab for routine
495 COVID diagnosis. Prior to using the rapid test, the nasopharyngeal swab samples were validated
496 by qRT-PCR using GeneFinder™ COVID-19 Plus Real*Amp* Kit (OSANGHealtcare, Anyang-si,
497 Gyeonggi-do, Republic of Korea I). The primary study under which the samples and data were
498 collected received ethical clearance from the Faculdade de Medicina de São José do Rio Preto
499 (FAMERP), protocol number 31588920.0.0000.5415. All excess samples and corresponding data
500 were banked and de-identified prior to the analyses.

501 Nasopharyngeal swab specimens (1 mL) were concentrated using Vivaspin 500 centrifugal
502 concentrator (Sartorius, Goettingen, Germany) at 12,000 x g for 10 minutes. The concentrated

503 nasopharyngeal swab specimen retentate was transferred to a collection tube and the rapid antigen
504 test for SARS-CoV-2 spike detection was inserted into the tube with the retentate and allowed to
505 react for 15 minutes. After processing of the rapid antigen test, the visual positive or negative
506 signal was documented.
507
508 **Data for Modeling**
509 As of August 2020, the United States and Brazil have the highest number of confirmed
510 COVID-19 cases and deaths worldwide, with both countries reporting their first case on 26
511 February 202) (*1*). Although several affected US regions could have been modeled, we look at
512 data from Massachusetts, New York, and Los Angeles: these regions each contained "hotspots",
513 or areas of surging COVID-19 cases, at different points in time during the pandemic and have
514 publicly available government-provided surveillance data. Our model is fit using data over 105
515 days beginning on April 1 for Figure 2 and 105 days beginning on April 10 for Figure 3 (see
516 "Modeling Parameters" in Methods). In order to understand the various testing proposals on a
517 global scale, we performed our clinical study in and expanded the modeling study to Brazil. The
518 specific data we use to fit our model are cumulative confirmed cases, total deaths, and number of
519 daily hospitalizations due to COVID-19. This surveillance data was retrieved from government-
520 provided online databases (*45–51*).
521
522 **Modeling Parameters**
523 Equation 2 below provides the exact differential equations governing the model.

$$
\begin{aligned}
\mathrm{d}\mathbf{S} &= & -\mathbf{S}\left(\alpha\mathbf{I}+\eta\mathbf{D}+\gamma\right) & & +\psi\mathbf{Q_U} \\
\mathrm{d}\mathbf{I} &= & -\mathbf{I}\left(\varepsilon+\lambda+\nu\right) & & +\mathbf{S}\left(\alpha\mathbf{I}+\eta\mathbf{D}\right) \\
\mathrm{d}\mathbf{D} &= & -\mathbf{D}\left(\frac{\mathbf{D}+\mathbf{I}}{\mathbf{D}}\mu+\rho\right) & & +\mathbf{I}(\nu+\varepsilon) \\
\mathrm{d}\mathbf{H} &= & -\mathbf{H}\left(\sigma+\tau\right) & & +\mu\left(\mathbf{D}+\mathbf{I}\right) \\
\mathrm{d}\mathbf{E} &= & & & +\tau\mathbf{H} \\
\mathrm{d}\mathbf{R} &= & -\gamma\mathbf{R} & & +\rho\mathbf{D}+\lambda\mathbf{I}+\sigma\mathbf{H}+\psi\mathbf{Q_R} \\
\mathrm{d}\mathbf{Q_U} &= & -\psi\mathbf{Q_U} & & +\gamma\mathbf{S} \\
\mathrm{d}\mathbf{Q_R} &= & -\psi\mathbf{Q_R} & & +\gamma\mathbf{R}
\end{aligned}
\tag{2}
$$

In order to determine the values of the parameters defining the flows between states, we use a least squares regression performed at seven day intervals in the datasets to which we fit. This allows the model to take into account the time dependent nature of the parameters, which rely on factors such as social distancing regulations and changes in testing capacity. We also fit window sizes between 1 and 21 days and find that while the fit degrades with larger window size, the overall shape of the fits do not change. We choose seven days assuming policy changes take a week to become effective and that reasonable parameters can be expected to change within this time period. Also, the seven day window size accounts for the fact that often data is not reported as diligently over the weekend. Time series of the values of the parameters for the geographic locations discussed in this paper are included in Figure S5.

Given the restrictions on data available for the populations of various states, varying all of the parameters results in an over parameterized system. Therefore, a subset of the model parameters are fit while the others are either extracted from other sources; see Table 3. The fitting procedure minimizes the sum of the squared residuals of the total cases, current daily hospitalizations, cumulative deaths, and percentage of total infected individuals currently hospitalized. The first three are present in the data sets while the latter is derived from the estimates of the ratio between infected undetected to infected detected individuals from the CDC Laboratory

542 Seroprevalence Survey Data (*52*). While this ratio changes over time, the percentage of infected
543 individuals developing severe symptoms should remain roughly constant throughout the course of
544 the epidemic in the different locations studied.

545 We consider the data sets for outbreaks in MA, NYC, LA, and SJRP, Brazil (*45–50*). While
546 each location has testing and fatality information dating back to January, hospitalization data was
547 not included until late March (for NYC and SJRP) and April (for MA and LA). Hence we begin
548 our fitting procedure and testing strategy on 1 April for each of the data sets; by this point, the
549 outbreak is advanced in NYC, substantial in MA, non-negligible, but far from its peak, in LA, and
550 in early stages in SJRP, Brazil. Starting simulations at various stages of the outbreak allows one
551 to see the difference in results between when a testing strategy is administered.

552 In order to determine the effectiveness of the county-based strategy when applied to the
553 state of California, we also fit all of the counties in California with a population greater than 1.5%
554 of that of the entire state and with greater than zero deaths. The results do not depend on these
555 selections, but instead suggest a practical criteria to administer limited resources. The fitting is
556 done starting 10 April for these counties, as at this point the outbreak is sufficiently well-
557 documented in each to successfully model. For the county-level data we compute a seven day
558 running average of each of the data sets to which we then fit in order to smooth out fluctuations in
559 the data, likely due to reporting, which are more significant here than in the other data sets
560 considered, as the county populations are smaller and hence discrepancies impact the smoothness
561 of the data more. The fits for each of the counties can be found in Figure S6.

562 As one can see from Figure 1, these data sets are particularly not smooth, which indicates
563 inefficiencies in reporting. Additionally, it is difficult to gauge their consistency within the dates
564 provided or to compare between locations, as reporting mechanisms changed over time within the

565 same locations. Despite this lack of consistency, our model and fitting mechanism was successful
566 in reproducing the progress of the outbreak in each data set studied.
567 The authors confirm that the data supporting the findings of this study are available within the
568 article and/or its supplementary materials; any other data will be made available upon request. Our
569 code can be found on github: https://github.com/badeaa3/COVID19_Rapid_Testing. The code is
570 written using python with the packages scipy, numpy, lmfit, matplotlib and plotly (*53–57*).

571 **Supplementary Materials**

572

573 **Table S1. Data summary of direct antigen rapid test (DART) for detection of SARS-CoV-2**
574 **nucleocapsid protein and DART for detection of SARS-CoV-2 spike glycoprotein**
575 **performance in comparison to qRT-PCR results.**

576

577 **Table S2. Summary of results of COVID-19 outcomes in 3 US Regions and Brazil as a result**
578 **of Frequent Rapid Testing Protocol using SIDHRE-Q Model.**

579

580 **Table S3. Demographic and clinical summary of patients evaluated by the SARS-CoV-2**
581 **Direct Antigen Rapid Test (DART).**

582

583 **Figure S1. Performance of direct antigen rapid test (DART) for the detection of SARS-**
584 **CoV-2 (A) nuceleocapsid protein and (B) spike glycoprotein.** Shown are the percentile
585 positive cases of the total positive population conditioned to qRT-PCR Cycle Threshold (Ct).

586 Percentile Positive ranks the samples in order of high Ct to low Ct. DART sensitivity is
587 determined by calculating true positive agreement to qRT-PCR; the plot uses an ax^b+c fit and
588 95% confidence intervals for the sensitivity.
589
590 **Figure S2. Graphical scheme displaying the relationships between the stages of quarantine**
591 **and infection in *SIDHRE-Q* model: Q-U**, quarantine uninfected; **S**, susceptible (uninfected); **I**,
592 infected undetected (pre-testing and infected); **D**, infected detected (infection diagnosis through
593 testing); **H**, hospitalized (infected with life threatening symptom progression); **R**, recovered
594 (healed); **E**, extinct (dead); and **Q-R**, quarantine recovered (healed but in quarantine by false
595 positive testing).
596
597 **Figure S3. COVID-19 Outcomes as a result of Frequent Rapid Testing Protocol with**
598 **variable test performances using *SIDHRE-Q* Model.** The Cumulative Detected Infected,
599 Hospitalized, Deceased, Active Infections, Recovered, and Quarantined are modeled over 105
600 days (top to bottom) using reported data from 4 global regions: Massachusetts, Los Angeles,
601 New York City, and São José do Rio Preto in Brazil (left to right). The COVID-19 population
602 spread and outcomes are modeled under a Rapid Testing Protocol with variable testing
603 frequencies ranging from 1-21 days between tests, and variable test performances: 90%
604 specificity with 90% sensitivity (A), 70% sensitivity (B), 50% sensitivity (C), and 30%
605 sensitivity (D); and 80% specificity with 90% sensitivity (E), 70% sensitivity (F), 50%
606 sensitivity (G), and 30% sensitivity (H). This protocol is compared to a symptom-based Rapid
607 Testing protocol and a symptom-based qRT-PCR protocol.
608

Figure S4. Effect of Rapid Testing Protocol under variable testing sensitivities and increasing frequency under the *SIDHRE-Q* Model. The Cumulative Infections, Maximum Simultaneously Hospitalized, and Deceased populations are modeled for Massachusetts, Los Angeles, New York City, and São José do Rio Preto in Brazil. The effect of increasing frequency of testing is modeled for various testing sensitivities (30%-90%) with an 80% specificity.

Figure S5. **Time series of the four fitted parameters α, ν, μ, and τ (left to right) for MA, LA, NYC, and SJRP (top to bottom).** See Table 2 in the Methods section for an explanation of the parameters. The values are extracted every seven days from data provided by the respective regions. The parameters vary significantly over time and location. Flat points occur during the seven day windows where the parameters are held constant. The fitting procedure is also outlined in the Methods section.

Figure S6. Time series of the three fitted pieces of data Cumulative Cases, Daily Hospitalized, and Cumulative Deaths (left to right) for each county receiving testing in CA; Ventura (2A), Stanislaus (2B), Santa Clara (2C), San Joaquin (2D), San Francisco (2E), San Diego (2F), San Bernardino (2G), Sacramento (2H), Orange (2I), Los Angeles (2J), Kern (2K), Fresno (2L), Alameda (2M). The counties included satisfy two requirements: population greater than 1.5% of the total CA population and nonzero total number of deaths at each point in time. The fitting procedure is outlined in the Methods section.

References

1. Coronavirus Disease (COVID-19) Situation Reports, (available at https://www.who.int/emergencies/diseases/novel-coronavirus-2019/situation-reports).

2. T. F. Menkir, T. Chin, J. A. Hay, E. Surface, P. Martinez de Salazar, C. Buckee, M. J. Mina, K. Khan, A. Watts, M. Lipsitch, R. Niehus, Estimating the number of undetected COVID-19 cases exported internationally from all of China. *medRxiv* (2020), doi:10.1101/2020.03.23.20038331.

3. B. Ivorra, M. R. Ferrández, M. Vela-Pérez, A. M. Ramos, Mathematical modeling of the spread of the coronavirus disease 2019 (COVID-19) taking into account the undetected infections. The case of China. *Commun Nonlinear Sci Numer Simul*, 105303 (2020).

4. M. Salathé, C. L. Althaus, R. Neher, S. Stringhini, E. Hodcroft, J. Fellay, M. Zwahlen, G. Senti, M. Battegay, A. Wilder-Smith, I. Eckerle, M. Egger, N. Low, COVID-19 epidemic in Switzerland: on the importance of testing, contact tracing and isolation. *Swiss Med Wkly*. **150**, w20225 (2020).

5. H. Lau, T. Khosrawipour, P. Kocbach, H. Ichii, J. Bania, V. Khosrawipour, Evaluating the massive underreporting and undertesting of COVID-19 cases in multiple global epicenters. *Pulmonology* (2020), doi:10.1016/j.pulmoe.2020.05.015.

649 6. J. D. Silverman, N. Hupert, A. D. Washburne, Using influenza surveillance networks to
650 estimate state-specific prevalence of SARS-CoV-2 in the United States. *Science*
651 *Translational Medicine* (2020), doi:10.1126/scitranslmed.abc1126.

652 7. D. Böhning, I. Rocchetti, A. Maruotti, H. Holling, Estimating the undetected infections in the
653 Covid-19 outbreak by harnessing capture-recapture methods. *Int. J. Infect. Dis.* **97**, 197–201
654 (2020).

655 8. Y. H. Baek, J. Um, K. J. C. Antigua, J.-H. Park, Y. Kim, S. Oh, Y. Kim, W.-S. Choi, S. G.
656 Kim, J. H. Jeong, B. S. Chin, H. D. G. Nicolas, J.-Y. Ahn, K. S. Shin, Y. K. Choi, J.-S. Park,
657 M.-S. Song, Development of a reverse transcription-loop-mediated isothermal amplification
658 as a rapid early-detection method for novel SARS-CoV-2. *Emerg Microbes Infect*. **9**, 998–
659 1007 (2020).

660 9. L. Leo, Mylab gets commercial approval from ICMR for Covid-19 antigen rapid testing kit.
661 *Livemint* (2020), (available at https://www.livemint.com/news/india/mylab-gets-commercial-
662 approval-from-icmr-for-covid-19-antigen-rapid-testing-kit-11595434040321.html).

663 10. S. Dey, Coronavirus testing: Rapid antigen tests now make up nearly half of daily checks |
664 India News - Times of India. *The Times of India*, (available at
665 https://timesofindia.indiatimes.com/india/rapid-antigen-tests-now-make-up-nearly-half-of-
666 daily-checks/articleshow/77340459.cms).

667 11. C. B. F. Vogels, A. F. Brito, A. L. Wyllie, J. R. Fauver, I. M. Ott, C. C. Kalinich, M. E.
668 Petrone, A. Casanovas-Massana, M. Catherine Muenker, A. J. Moore, J. Klein, P. Lu, A. Lu-
669 Culligan, X. Jiang, D. J. Kim, E. Kudo, T. Mao, M. Moriyama, J. E. Oh, A. Park, J. Silva, E.

670 Song, T. Takahashi, M. Taura, M. Tokuyama, A. Venkataraman, O.-E. Weizman, P. Wong,
671 Y. Yang, N. R. Cheemarla, E. B. White, S. Lapidus, R. Earnest, B. Geng, P. Vijayakumar, C.
672 Odio, J. Fournier, S. Bermejo, S. Farhadian, C. S. Dela Cruz, A. Iwasaki, A. I. Ko, M. L.
673 Landry, E. F. Foxman, N. D. Grubaugh, Analytical sensitivity and efficiency comparisons of
674 SARS-CoV-2 RT-qPCR primer-probe sets. *Nat Microbiol* (2020), doi:10.1038/s41564-020-
675 0761-6.

676 12. D. B. Larremore, B. Wilder, E. Lester, S. Shehata, J. M. Burke, J. A. Hay, M. Tambe, M. J.
677 Mina, R. Parker, Test sensitivity is secondary to frequency and turnaround time for COVID-
678 19 surveillance. *medRxiv* (2020), doi:10.1101/2020.06.22.20136309.

679 13. Z. Shen, F. Ning, W. Zhou, X. He, C. Lin, D. P. Chin, Z. Zhu, A. Schuchat, Superspreading
680 SARS events, Beijing, 2003. *Emerging Infect. Dis.* **10**, 256–260 (2004).

681 14. J. S. M. Peiris, C. M. Chu, V. C. C. Cheng, K. S. Chan, I. F. N. Hung, L. L. M. Poon, K. I.
682 Law, B. S. F. Tang, T. Y. W. Hon, C. S. Chan, K. H. Chan, J. S. C. Ng, B. J. Zheng, W. L.
683 Ng, R. W. M. Lai, Y. Guan, K. Y. Yuen, HKU/UCH SARS Study Group, Clinical
684 progression and viral load in a community outbreak of coronavirus-associated SARS
685 pneumonia: a prospective study. *Lancet*. **361**, 1767–1772 (2003).

686 15. X. He, E. H. Y. Lau, P. Wu, X. Deng, J. Wang, X. Hao, Y. C. Lau, J. Y. Wong, Y. Guan, X.
687 Tan, X. Mo, Y. Chen, B. Liao, W. Chen, F. Hu, Q. Zhang, M. Zhong, Y. Wu, L. Zhao, F.
688 Zhang, B. J. Cowling, F. Li, G. M. Leung, Temporal dynamics in viral shedding and
689 transmissibility of COVID-19. *Nat. Med.* **26**, 672–675 (2020).

690 16. J. Bullard, K. Dust, D. Funk, J. E. Strong, D. Alexander, L. Garnett, C. Boodman, A. Bello,
691 A. Hedley, Z. Schiffman, K. Doan, N. Bastien, Y. Li, P. G. Van Caeseele, G. Poliquin,
692 Predicting infectious SARS-CoV-2 from diagnostic samples. *Clin. Infect. Dis.* (2020),
693 doi:10.1093/cid/ciaa638.

694 17. G. Giordano, F. Blanchini, R. Bruno, P. Colaneri, A. Di Filippo, A. Di Matteo, M. Colaneri,
695 Modelling the COVID-19 epidemic and implementation of population-wide interventions in
696 Italy. *Nat. Med.* **26**, 855–860 (2020).

697 18. S. Choi, M. Ki, Estimating the reproductive number and the outbreak size of COVID-19 in
698 Korea. *Epidemiol Health*. **42**, e2020011 (2020).

699 19. Y. Y. Wei, Z. Z. Lu, Z. C. Du, Z. J. Zhang, Y. Zhao, S. P. Shen, B. Wang, Y. T. Hao, F.
700 Chen, [Fitting and forecasting the trend of COVID-19 by SEIR(+CAQ) dynamic model].
701 *Zhonghua Liu Xing Bing Xue Za Zhi*. **41**, 470–475 (2020).

702 20. Z. Yang, Z. Zeng, K. Wang, S.-S. Wong, W. Liang, M. Zanin, P. Liu, X. Cao, Z. Gao, Z.
703 Mai, J. Liang, X. Liu, S. Li, Y. Li, F. Ye, W. Guan, Y. Yang, F. Li, S. Luo, Y. Xie, B. Liu,
704 Z. Wang, S. Zhang, Y. Wang, N. Zhong, J. He, Modified SEIR and AI prediction of the
705 epidemics trend of COVID-19 in China under public health interventions. *J Thorac Dis*. **12**,
706 165–174 (2020).

707 21. S. Cao, P. Feng, P. Shi, [Study on the epidemic development of COVID-19 in Hubei
708 province by a modified SEIR model]. *Zhejiang Da Xue Xue Bao Yi Xue Ban*. **49**, 178–184
709 (2020).

22. R. Huang, M. Liu, Y. Ding, Spatial-temporal distribution of COVID-19 in China and its prediction: A data-driven modeling analysis. *J Infect Dev Ctries*. **14**, 246–253 (2020).

23. A. Godio, F. Pace, A. Vergnano, SEIR Modeling of the Italian Epidemic of SARS-CoV-2 Using Computational Swarm Intelligence. *Int J Environ Res Public Health*. **17** (2020), doi:10.3390/ijerph17103535.

24. M. Gatto, E. Bertuzzo, L. Mari, S. Miccoli, L. Carraro, R. Casagrandi, A. Rinaldo, Spread and dynamics of the COVID-19 epidemic in Italy: Effects of emergency containment measures. *Proc. Natl. Acad. Sci. U.S.A.* **117**, 10484–10491 (2020).

25. C. Hou, J. Chen, Y. Zhou, L. Hua, J. Yuan, S. He, Y. Guo, S. Zhang, Q. Jia, C. Zhao, J. Zhang, G. Xu, E. Jia, The effectiveness of quarantine of Wuhan city against the Corona Virus Disease 2019 (COVID-19): A well-mixed SEIR model analysis. *J. Med. Virol.* **92**, 841–848 (2020).

26. T. Zhou, Q. Liu, Z. Yang, J. Liao, K. Yang, W. Bai, X. Lu, W. Zhang, Preliminary prediction of the basic reproduction number of the Wuhan novel coronavirus 2019-nCoV. *J Evid Based Med*. **13**, 3–7 (2020).

27. C. Reno, J. Lenzi, A. Navarra, E. Barelli, D. Gori, A. Lanza, R. Valentini, B. Tang, M. P. Fantini, Forecasting COVID-19-Associated Hospitalizations under Different Levels of Social Distancing in Lombardy and Emilia-Romagna, Northern Italy: Results from an Extended SEIR Compartmental Model. *J Clin Med*. **9** (2020), doi:10.3390/jcm9051492.

729 28. F. Yu, L. Yan, N. Wang, S. Yang, L. Wang, Y. Tang, G. Gao, S. Wang, C. Ma, R. Xie, F.
730 Wang, C. Tan, L. Zhu, Y. Guo, F. Zhang, Quantitative Detection and Viral Load Analysis of
731 SARS-CoV-2 in Infected Patients. *Clin. Infect. Dis.* **71**, 793–798 (2020).

732 29. S. N. Rao, D. Manissero, V. R. Steele, J. Pareja, A Narrative Systematic Review of the
733 Clinical Utility of Cycle Threshold Values in the Context of COVID-19. *Infect Dis Ther*, 1–
734 14 (2020).

735 30. J. Alizargar, Risk of reactivation or reinfection of novel coronavirus (COVID-19). *J.*
736 *Formos. Med. Assoc.* **119**, 1123 (2020).

737 31. D. Batisse, N. Benech, E. Botelho-Nevers, K. Bouiller, R. Collarino, A. Conrad, L. Gallay,
738 F. Goehringer, M. Gousseff, D. C. Joseph, A. Lemaignen, F.-X. Lescure, B. Levy, M.
739 Mahevas, P. Penot, B. Pozzetto, D. Salmon, D. Slama, N. Vignier, B. Wyplosz, Clinical
740 recurrences of COVID-19 symptoms after recovery: viral relapse, reinfection or
741 inflammatory rebound? *J. Infect.* (2020), doi:10.1016/j.jinf.2020.06.073.

742 32. W. Deng, L. Bao, J. Liu, C. Xiao, J. Liu, J. Xue, Q. Lv, F. Qi, H. Gao, P. Yu, Y. Xu, Y. Qu,
743 F. Li, Z. Xiang, H. Yu, S. Gong, M. Liu, G. Wang, S. Wang, Z. Song, Y. Liu, W. Zhao, Y.
744 Han, L. Zhao, X. Liu, Q. Wei, C. Qin, Primary exposure to SARS-CoV-2 protects against
745 reinfection in rhesus macaques. *Science* (2020), doi:10.1126/science.abc5343.

746 33. M. Ota, Will we see protection or reinfection in COVID-19? *Nat. Rev. Immunol.* **20**, 351
747 (2020).

748 34. A. Victor Okhuese, Estimation of the Probability of Reinfection With COVID-19 by the
749 Susceptible-Exposed-Infectious-Removed-Undetectable-Susceptible Model. *JMIR Public*
750 *Health Surveill*. **6**, e19097 (2020).

751 35. Y. Gu, COVID-19 Projections Using Machine Learning. *COVID-19 Projections Using*
752 *Machine Learning*, (available at https://covid19-projections.com/).

753 36. D. Stadlbauer, J. Tan, K. Jiang, M. Hernandez, S. Fabre, F. Amanat, C. Teo, G. A.
754 Arunkumar, M. McMahon, J. Jhang, M. Nowak, V. Simon, E. Sordillo, H. van Bakel, F.
755 Krammer, *medRxiv*, in press, doi:10.1101/2020.06.28.20142190.

756 37. A. Goodnough, M. D. Shear, The U.S.'s Slow Start to Coronavirus Testing: A Timeline. *The*
757 *New York Times* (2020), (available at https://www.nytimes.com/2020/03/28/us/coronavirus-
758 testing-timeline.html).

759 38. M. D. Shear, A. Goodnough, S. Kaplan, S. Fink, K. Thomas, N. Weiland, The Lost Month:
760 How a Failure to Test Blinded the U.S. to Covid-19. *The New York Times* (2020), (available
761 at https://www.nytimes.com/2020/03/28/us/testing-coronavirus-pandemic.html).

762 39. S. Kaplan, K. Thomas, Despite Promises, Testing Delays Leave Americans 'Flying Blind.'
763 *The New York Times* (2020), (available at
764 https://www.nytimes.com/2020/04/06/health/coronavirus-testing-us.html).

765 40. W. M. de Souza, L. F. Buss, D. da S. Candido, J.-P. Carrera, S. Li, A. E. Zarebski, R. H. M.
766 Pereira, C. A. Prete, A. A. de Souza-Santos, K. V. Parag, M. C. T. D. Belotti, M. F.
767 Vincenti-Gonzalez, J. Messina, F. C. da Silva Sales, P. dos S. Andrade, V. H. Nascimento, F.
768 Ghilardi, L. Abade, B. Gutierrez, M. U. G. Kraemer, C. K. V. Braga, R. S. Aguiar, N.

Alexander, P. Mayaud, O. J. Brady, I. Marcilio, N. Gouveia, G. Li, A. Tami, S. B. de Oliveira, V. B. G. Porto, F. Ganem, W. A. F. de Almeida, F. F. S. T. Fantinato, E. M. Macário, W. K. de Oliveira, M. L. Nogueira, O. G. Pybus, C.-H. Wu, J. Croda, E. C. Sabino, N. R. Faria, Epidemiological and clinical characteristics of the COVID-19 epidemic in Brazil. *Nature Human Behaviour*. **4**, 856–865 (2020).

41. S. Mervosh, M. Fernandez, 'It's Like Having No Testing': Coronavirus Test Results Are Still Delayed. *The New York Times* (2020), (available at https://www.nytimes.com/2020/08/04/us/virus-testing-delays.html).

42. K. Gostic, A. C. Gomez, R. O. Mummah, A. J. Kucharski, J. O. Lloyd-Smith, Estimated effectiveness of symptom and risk screening to prevent the spread of COVID-19. *eLife*. **9**, e55570 (2020).

43. T. Zitek, The Appropriate Use of Testing for COVID-19. *West J Emerg Med*. **21**, 470–472 (2020).

44. I. Bosch, H. de Puig, M. Hiley, M. Carré-Camps, F. Perdomo-Celis, C. F. Narváez, D. M. Salgado, D. Senthoor, M. O'Grady, E. Phillips, A. Durbin, D. Fandos, H. Miyazaki, C.-W. Yen, M. Gélvez-Ramírez, R. V. Warke, L. S. Ribeiro, M. M. Teixeira, R. P. Almeida, J. E. Muñóz-Medina, J. E. Ludert, M. L. Nogueira, T. E. Colombo, A. C. B. Terzian, P. T. Bozza, A. S. Calheiros, Y. R. Vieira, G. Barbosa-Lima, A. Vizzoni, J. Cerbino-Neto, F. A. Bozza, T. M. L. Souza, M. R. O. Trugilho, A. M. B. de Filippis, P. C. de Sequeira, E. T. A. Marques, T. Magalhaes, F. J. Díaz, B. N. Restrepo, K. Marín, S. Mattar, D. Olson, E. J. Asturias, M. Lucera, M. Singla, G. R. Medigeshi, N. de Bosch, J. Tam, J. Gómez-Márquez, C. Clavet, L.

790 Villar, K. Hamad-Schifferli, L. Gehrke, Rapid antigen tests for dengue virus serotypes and
791 Zika virus in patient serum. *Sci Transl Med*. **9** (2017), doi:10.1126/scitranslmed.aan1589.

792 45. Massachusetts Department of Public Health, COVID-19 Response Reporting. *Mass.gov*,
793 (available at https://www.mass.gov/info-details/covid-19-response-reporting).

794 46. California Department of Public Health, COVID-19 Cases - California Open Data, (available
795 at https://data.ca.gov/dataset/covid-19-cases).

796 47. California Department of Public Health, COVID-19 Hospital Data - California Open Data,
797 (available at https://data.ca.gov/dataset/covid-19-hospital-data).

798 48. Department of Health and Human Hygiene, COVID-19 Daily Counts of Cases,
799 Hospitalizations, and Deaths | NYC Open Data, (available at
800 https://data.cityofnewyork.us/Health/COVID-19-Daily-Counts-of-Cases-Hospitalizations-
801 an/rc75-m7u3).

802 49. Sao Jose do Rio Preto Public Health Office, "COVID-19 Surveillance Data, Sao Jose do Rio
803 Preto" (Sao Jose do Rio Preto Public Health Office, Sao Jose do Rio Preto, Brazil).

804 50. New York State Government, Daily Hospitalization Summary by Region. *New York*
805 *Forward*, (available at https://forward.ny.gov/daily-hospitalization-summary-region).

806 51. Massachusetts General Hospital Institute for Technology Assessment, COVID-19 Simulator
807 - Methodology, (available at https://www.covid19sim.org/images/docs/COVID-
808 19_simulator_methodology_download_20200507.pdf).

52. CDC, Coronavirus Disease 2019 (COVID-19). *Centers for Disease Control and Prevention* (2020), (available at https://www.cdc.gov/coronavirus/2019-ncov/cases-updates/commercial-lab-surveys.html).

53. SciPy.org — SciPy.org, (available at https://www.scipy.org/).

54. NumPy, (available at https://numpy.org/).

55. Non-Linear Least-Squares Minimization and Curve-Fitting for Python — Non-Linear Least-Squares Minimization and Curve-Fitting for Python, (available at https://lmfit.github.io/lmfit-py/).

56. Matplotlib: Python plotting — Matplotlib 3.3.1 documentation, (available at https://matplotlib.org/).

57. Plotly: The front-end for ML and data science models, (available at https://plotly.com/).

Acknowledgments

General: We thank Professor Lee Gehrke for critical reading of the manuscript.

Funding: EN is funded by Tufts University DISC Seed Grant. MLN is supported by a FAPESP grant (#2020/04836-0) and is a CNPq Research Fellow. AFV is supported by a FAPESP Fellow grant (#18/17647-0). GRFC is supported by a FAPESP Fellow grant (#20/07419-0). BHGAM is supported by a FAPESP Scholarship (#19/06572-2). The funders had no role in the design of the study; in the collection, analyses, or interpretation of data; in the writing of the manuscript, or in the decision to publish the results.

830 **Author contributions:** Conceptualization: BBH. Formal analysis: BN, AB, AR, MB,
831 NS, ARG, AV, GCDS, TMILDS, BHGAM, MMM, GRFC, FQ, AFNR, MLG, ENN, IB,
832 BBH. Funding acquisition: IB, BBH. Investigation: BN, AB, AR, MB, NS, ARG, AV,
833 GCDS, TMILDS, BHGAM, MMM, GRFC, FQ, AFNR, MLG, ENN, IB, BBH.
834 Methodology: BN, AB, AR, MB, NS, ARG, AV, GCDS, TMILDS, BHGAM, MMM,
835 GRFC, FQ, AFNR, MLG, ENN, IB, BBH. Project administration: MLN, IB, BBH.
836 Resources: MLN, IB, BBH. Supervision: MB, MLN, ENN, IB, BBH. Validation: BN,
837 AB, AR, MB, ENN, BBH. Visualization: BN, AB, AR, MB, AV, ENN, BBH. Writing—
838 original draft: AR, BBH. Writing—review and editing: BN, AB, AR, MB, NS, ARG,
839 AV, GCDS, TMILDS, BHGAM, MMM, GRFC, FQ, AFNR, MLG, ENN, IB, BBH.
840 **Competing interests:** BN, AB, AR, MB, NS, AG, IB, and BBH are employed by or
841 affiliated with E25Bio Inc. (www.e25bio.com), a company that develops diagnostics for
842 epidemic viruses.
843
844
845 **Figures and Tables**
846
847 **TABLES**
848
849 **Table 1. Clinical validation summary for the direct antigen rapid test (DART) for SARS-**
850 **CoV-2 nucleocapsid protein evaluated using 190 retrospectively collected patient nasal**
851 **swab specimens.**
852

All Data Summary								
		qRT-PCR (gene average)					95% Confidence Interval	
		+	-	Total	Sensitivity	80.0%	76.1%	83.9%
DART (nucleocapsid protein)	+	80	8	88	Specificity	91.1%	88.2%	94.0%
	-	20	82	102	Positive Predictive Value	90.9%	87.9%	93.9%
	Total	100	90	190	Negative Predictive Value	80.4%	76.6%	84.2%
					Prevalence	52.6%	47.8%	57.5%
					Overall Agreement	85.3%	82.8%	87.8%

Table 2. Clinical validation summary for the SARS-CoV-2 direct antigen rapid test (DART) for SARS-SoC-2 spike glycoprotein evaluated using 121 retrospectively collected patient nasopharyngeal swab specimens.

All Data Summary								
		qRT-PCR (gene average)					95% Confidence Interval	
		+	-	Total	Sensitivity	84.7%	80.6%	88.9%
DART (spike glycoprotein)	+	61	7	68	Specificity	85.7%	80.8%	90.6%
	-	11	42	53	Positive Predictive Value	89.7%	86.2%	93.2%
	Total	72	49	121	Negative Predictive Value	79.2%	73.6%	84.9%
					Prevalence	59.5%	53.9%	65.1%
					Overall Agreement	85.1%	82.0%	88.3%

Table 3. Details of parameter values used for *SIDHRE-Q* Model.

Parameter	Details & Statistics			
	α is the probability that an interaction between an undetected infected person and		Mean	St. Dev.

α	an uninfected person results in a new infection, divided by the average number of uninfected people an undetected infected person comes into contact with on a given day. $\alpha$is estimated from the data.	MA	0.088	0.051
		LA	0.090	0.034
		NYC	0.067	0.042
		SJRP	0.121	0.042
η	$\eta$is the probability that an interaction between an infected person and an uninfected person results in a new infection, divided by the average number of uninfected people a detected infected person comes into contact with on a given day.$\eta = 0.01 \cdot \alpha$ The constant relating η, α accounts for a small but nonzero transmission due to the quarantined (detected) infected population. This value was chosen to be small, assuming a quarantined individual will only infect others with low probability.			
ν	$\nu$is the probability that a symptomatic undetected individual is diagnosed on a given day. $\nu$is estimated from the data. $\nu$is multiplied by sensitivity (assume benchmark sensitivity 100% for PCR, as used when fitting).		Mean	St. Dev.
		MA	0.006	0.005
		LA	0.011	0.006
		NYC	0.0056	0.002
		SJRP	0.015	0.007
ϵ	ϵ is the probability that an asymptomatic undetected infected individual is diagnosed on a given day. $\epsilon = 0$ while fitting (during PCR symptomatic testing). ϵ =(sensitivity/days between tests) when the rapid testing strategy is activated.			
λ	λ is the probability that an undetected infected individual transitions to the recovered state on a given day. $\lambda = 1/14$, or the inverse of average recovery time (*51*).			
μ	μ is the probability that an infected individual develops severe symptoms on a given day and transitions into the hospitalized state. The flow from D to H is assumed to be independent of the ratio I/D, but comes only from the detected infected population, hence why it is multiplied by $(I + D)/D$. μ is estimated from the data.		Mean	St. Dev.
		MA	0.0013	9.5e-4
		LA	0.0016	2.4e-4
		NYC	0.0011	6.6e-4
		SJRP	0.0018	8.0e-4
ρ	$\rho$is the probability that a detected infected individual transitions to the recovered state on a given day. $\rho = 1/14$, or the inverse of the average recovery time (*51*).			
σ	$\sigma$is the probability that a hospitalized individual transitions to the recovered state on a given day. $\sigma = 1/11$, or the inverse of the average recovery time for a hospitalized individual (*51*).			
τ	τ is the probability that a hospitalized individual expires on a given day. τ is estimated from the data.		Mean	St. Dev.
		MA	0.034	0.012

		LA	0.016	0.004
		NYC	0.036	0.034
		SJRP	0.032	0.045
γ	γ is the probability of entering either of the quarantine states on a given day from either the Susceptible or Recovered populations. $\gamma = 0$ while fitting (during PCR symptomatic testing). $\gamma = (1 - \text{specificity}) \times (1/\text{days between tests})$ when the rapid testing strategy is activated.			
ψ	ψ is the probability that an individual exits quarantine on a given day. $\psi = 1/14$, or the inverse of the quarantine period for fixed length quarantine.			
Parameter	Details & Statistics			
α	α is the probability that an interaction between an undetected infected person and an uninfected person results in a new infection, divided by the average number of uninfected people an undetected infected person comes into contact with on a given day. α is estimated from the data.		Mean	St. Dev.
		MA	0.088	0.051
		LA	0.090	0.034
		NYC	0.067	0.042
		SJRP	0.121	0.042
η	η is the probability that an interaction between an infected person and an uninfected person results in a new infection, divided by the average number of uninfected people a detected infected person comes into contact with on a given day. $\eta = 0.01 \cdot \alpha$ The constant relating η, α accounts for a small but nonzero transmission due to the quarantined (detected) infected population. This value was chosen to be small, assuming a quarantined individual will only infect others with low probability.			
ν	ν is the probability that a symptomatic undetected individual is diagnosed on a given day. ν is estimated from the data. ν is multiplied by sensitivity (assume benchmark sensitivity 100% for PCR, as used when fitting).		Mean	St. Dev.
		MA	0.006	0.005
		LA	0.011	0.006
		NYC	0.0056	0.002
		SJRP	0.015	0.007
ϵ	ϵ is the probability that an asymptomatic undetected infected individual is diagnosed on a given day. $\epsilon = 0$ while fitting (during PCR symptomatic testing). $\epsilon =$ (sensitivity/days between tests) when the rapid testing strategy is activated.			
λ	λ is the probability that an undetected infected individual transitions to the recovered state on a given day. $\lambda = 1/14$, or the inverse of average recovery time (*51*).			
μ	μ is the probability that an infected individual develops severe symptoms on a		Mean	St. Dev.

	given day and transitions into the hospitalized state. The flow from D to H is assumed to be independent of the ratio I/D, but comes only from the detected infected population, hence why it is multiplied by $(I+D)/D$. μ is estimated from the data.	MA	0.0013	9.5e-4
		LA	0.0016	2.4e-4
		NYC	0.0011	6.6e-4
		SJRP	0.0018	8.0e-4
ρ	ρ is the probability that a detected infected individual transitions to the recovered state on a given day. $\rho = 1/14$, or the inverse of the average recovery time (*51*).			
σ	σ is the probability that a hospitalized individual transitions to the recovered state on a given day. $\sigma = 1/11$, or the inverse of the average recovery time for a hospitalized individual (*51*).			
τ	τ is the probability that a hospitalized individual expires on a given day. τ is estimated from the data.		Mean	St. Dev.
		MA	0.034	0.012
		LA	0.016	0.004
		NYC	0.036	0.034
		SJRP	0.032	0.045
γ	γ is the probability of entering either of the quarantine states on a given day from either the Susceptible or Recovered populations. $\gamma = 0$ while fitting (during PCR symptomatic testing). $\gamma = (1 - \text{specificity}) \times (1/\text{days between tests})$ when the rapid testing strategy is activated.			
ψ	ψ is the probability that an individual exits quarantine on a given day. $\psi = 1/14$, or the inverse of the quarantine period for fixed length quarantine.			

FIGURES

Figure 1. Graphical scheme displaying the relationships between the stages of quarantine and infection in *SIDHRE-Q* model. **Q-U**, quarantine uninfected; **S**, susceptible (uninfected); **I**, infected undetected (pre-testing and infected); **D**, infected detected (infection diagnosis through

testing); **H**, hospitalized (infected with life threatening symptom progression); **R**, recovered (healed); **E**, extinct (dead); and **Q-R**, quarantine recovered (healed but in quarantine by false positive testing).

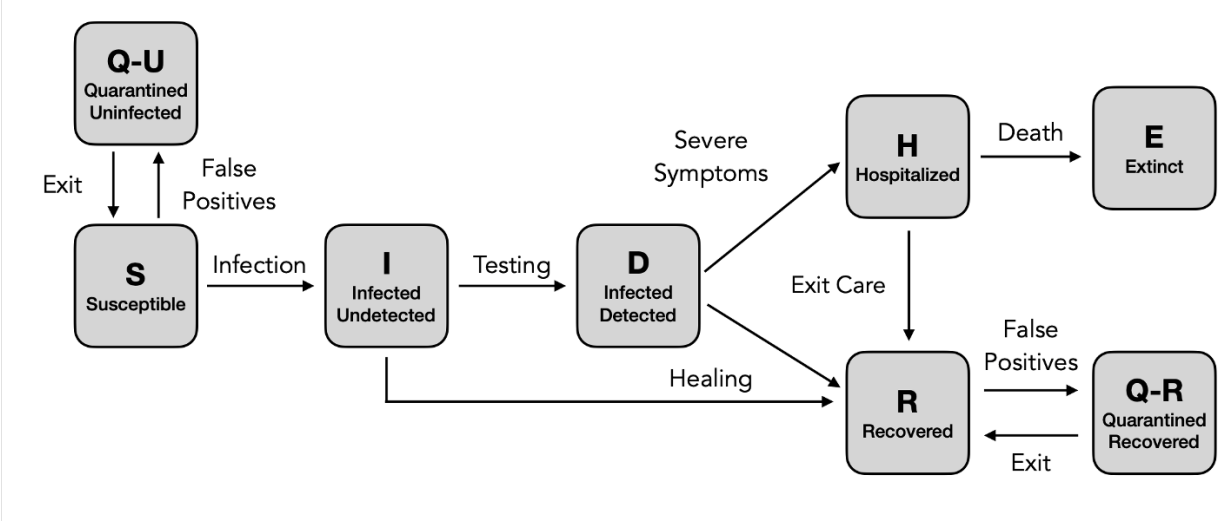

Figure 2. COVID-19 Outcomes in 3 US Regions and Brazil as a result of Frequent Rapid Testing Protocol using the *SIDHRE-Q* Model. (A) The Cumulative Detected Infected, Hospitalized, Deceased, Active Infections, Recovered, and Quarantined are modeled over 105 days (top to bottom) using reported data from 4 global regions: Massachusetts, Los Angeles, New York City, and São José do Rio Preto in Brazil (left to right). The COVID-19 population

905 spread and outcomes are modeled under a Rapid Testing Protocol (sensitivity 80%, specificity
906 90%) with variable testing frequencies ranging from 1-21 days between tests. This protocol is
907 compared to a symptom-based Rapid Testing protocol and a symptom-based PCR protocol. (B)
908 Effect of Rapid Testing Protocol under variable testing sensitivities (30%-90%) and increasing
909 frequency under the *SIDHRE-Q* Model. The Cumulative Infections, Maximum Simultaneously
910 Hospitalized, and Deceased populations are modeled for Massachusetts, Los Angeles, New York
911 City, and São José do Rio Preto in Brazil with a 90% test specificity.
912
913
914
915
916
917
918
919
920
921
922
923 **(A)**

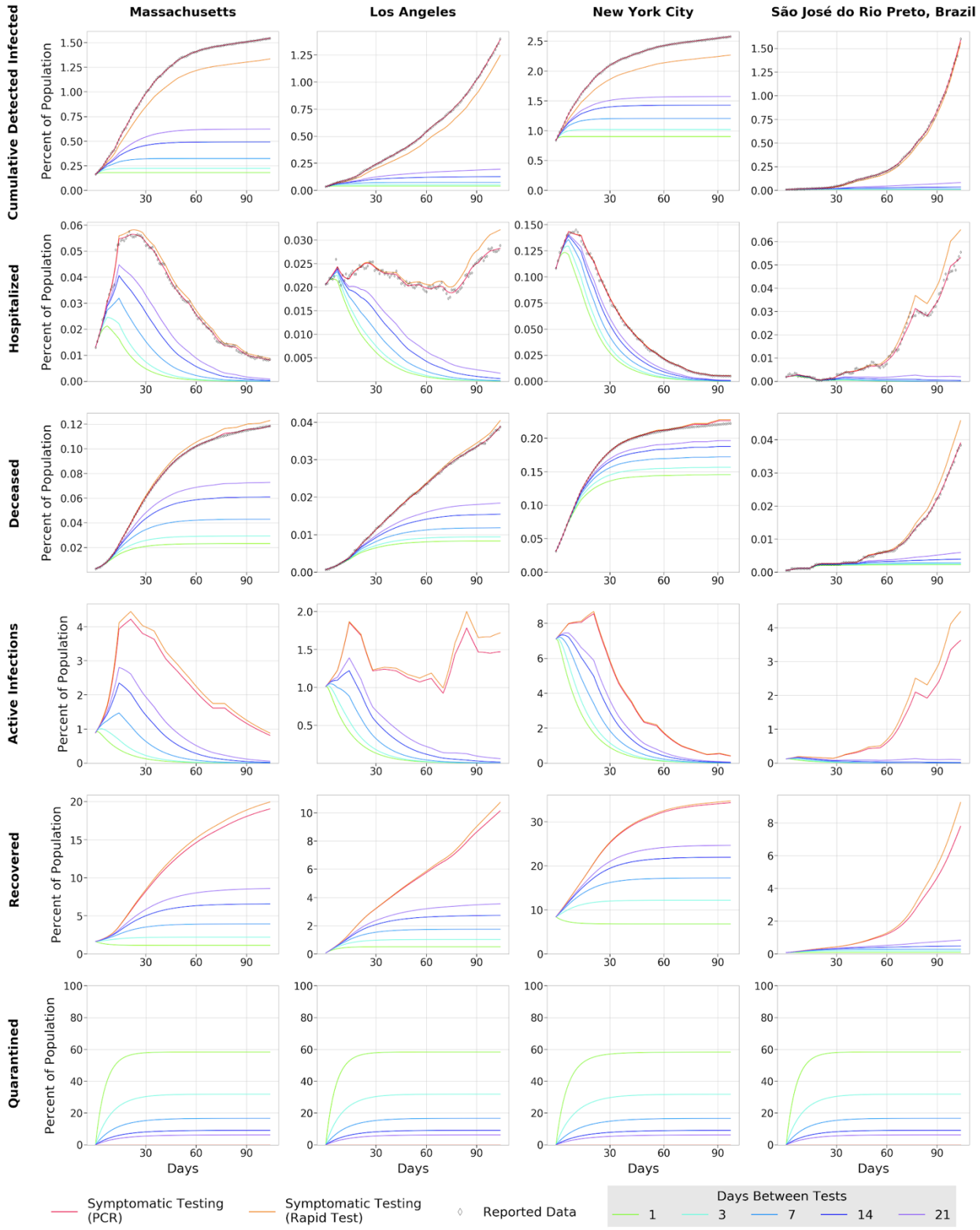
Massachusetts
Los Angeles
New York City
São José do Rio Preto, Brazil
Cumulative Detected Infected
Hospitalized
Deceased
Active Infections
Recovered
Quarantined
Percent of Population
Days
Symptomatic Testing (PCR)
Symptomatic Testing (Rapid Test)
Reported Data
Days Between Tests
1
3
7
14
21
Sensitivity: 80.0% Specificity: 90.0%

(B)

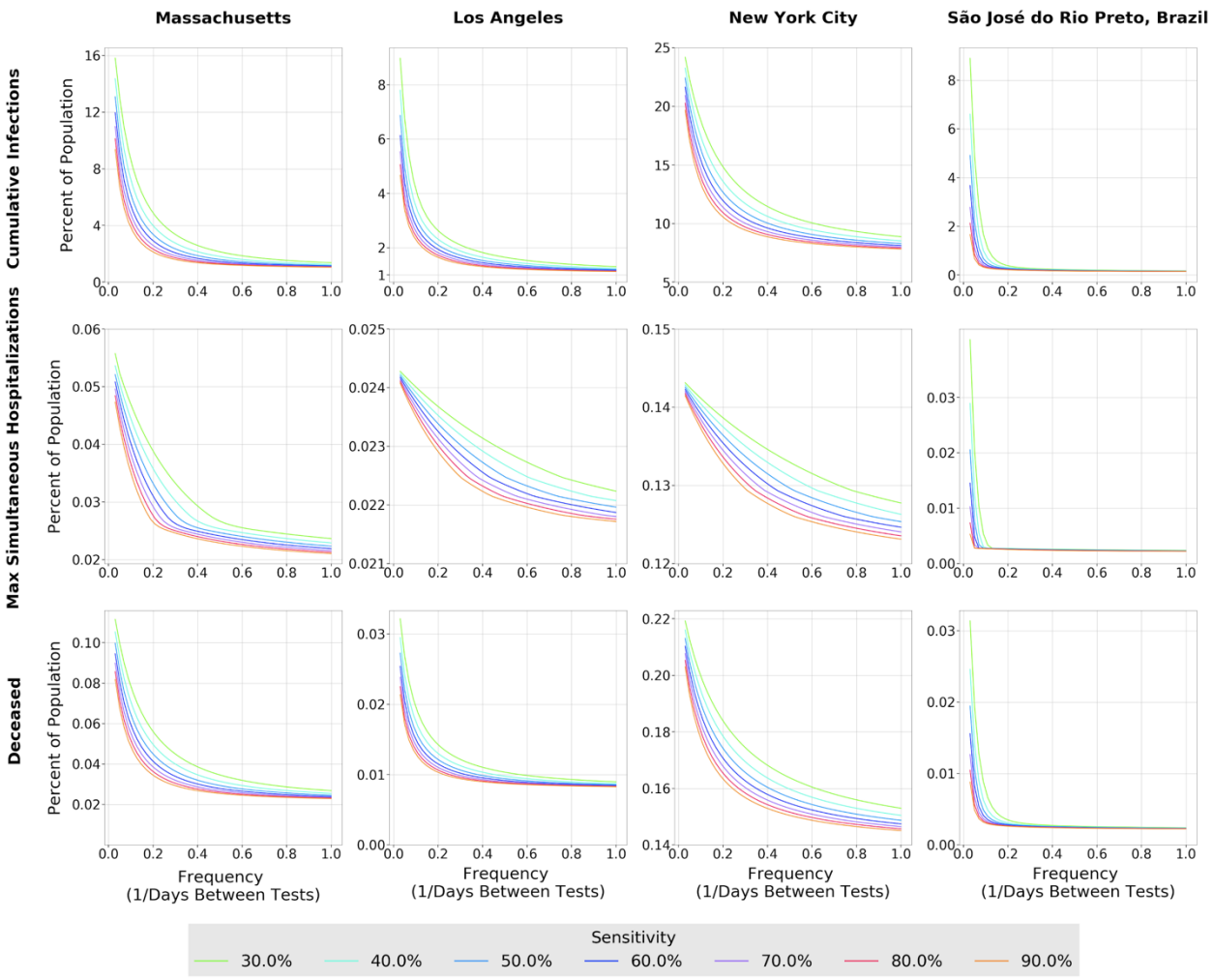

Specificity: 90.0%

Figure 3. Effect of County Based Rapid Testing strategy on COVID-19 outcomes in California. This protocol varies testing frequency in accordance to the number of recorded cases; the threshold for number of active infections which, if reached, signals to commence everyday testing (the highest frequency considered). A Rapid Test with a 80% sensitivity and 90% sensitivity versus is used in this deployment strategy. Shown is the total cost per person per day versus the cumulative infections, maximum simultaneously hospitalized, and cumulative deaths with varied thresholds for all of CA is shown. The County Based Rapid Testing strategy is compared to uniform testing, which distributes the same number of total tests used in the county strategy, albeit evenly across each county. The effects of uniform testing are modeled for both a Rapid Testing protocol and a qRT-PCR protocol (A). The effects of County Based Rapid Test Protocol and Uniform PCR Protocol on active infected detected population over time in CA are shown (B). The legend denotes the thresholds at which testing frequency is determined, the testing frequencies, the percent of CA population under the strategy, and the cost per person per day.

(A)

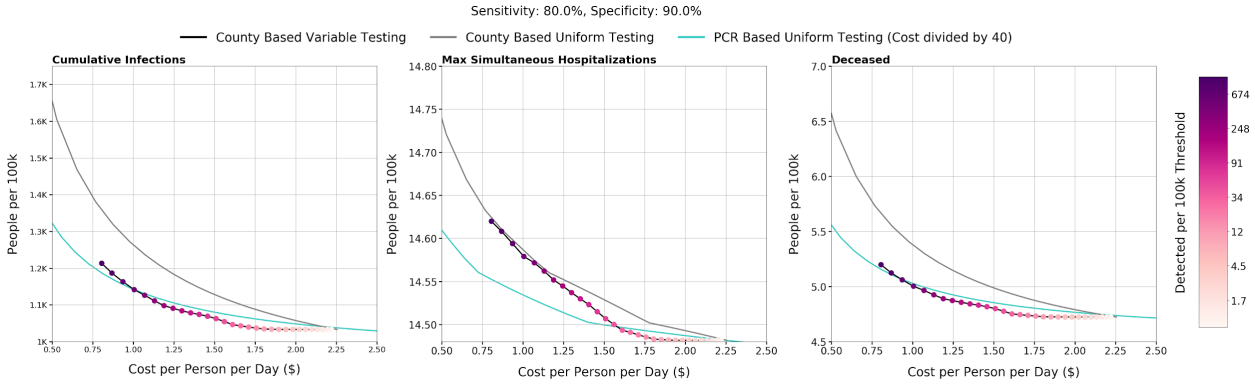

954 **(B)**

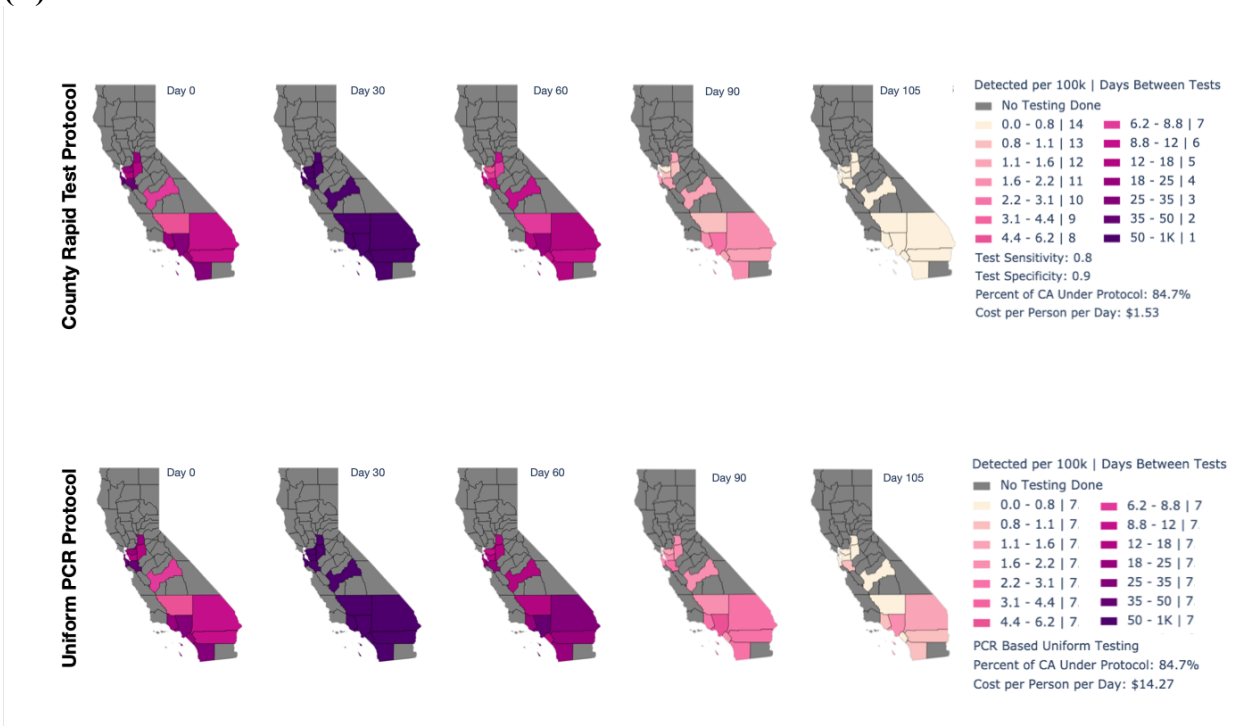
County Rapid Test Protocol
Day 0
Day 30
Day 60
Day 90
Day 105
Detected per 100k | Days Between Tests
No Testing Done
0.0 - 0.8 | 14
0.8 - 1.1 | 13
1.1 - 1.6 | 12
1.6 - 2.2 | 11
2.2 - 3.1 | 10
3.1 - 4.4 | 9
4.4 - 6.2 | 8
6.2 - 8.8 | 7
8.8 - 12 | 6
12 - 18 | 5
18 - 25 | 4
25 - 35 | 3
35 - 50 | 2
50 - 1K | 1
Test Sensitivity: 0.8
Test Specificity: 0.9
Percent of CA Under Protocol: 84.7%
Cost per Person per Day: $1.53
Uniform PCR Protocol
Day 0
Day 30
Day 60
Day 90
Day 105
Detected per 100k | Days Between Tests
No Testing Done
0.0 - 0.8 | 7
0.8 - 1.1 | 7
1.1 - 1.6 | 7
1.6 - 2.2 | 7
2.2 - 3.1 | 7
3.1 - 4.4 | 7
4.4 - 6.2 | 7
6.2 - 8.8 | 7
8.8 - 12 | 7
12 - 18 | 7
18 - 25 | 7
25 - 35 | 7
35 - 50 | 7
50 - 1K | 7
PCR Based Uniform Testing
Percent of CA Under Protocol: 84.7%
Cost per Person per Day: $14.27

955